[8] L. Lewin, *Theory of Waveguides. Techniques for the Solution of Waveguide Problems*, London, U.K.: Newnes-Butterworths, 1975.
[9] M. V. Davidovich, "Gap impedance characteristics for microstrip vibrator antenna," *Telecommun. Radio Eng.*, vol. 34, no. 6, pp. 68–71, June 1990 (in Russian).
[10] F. Bolinder, "Fourier transforms in the theory of inhomogeneous transmission lines," *Proc. IRE* , vol. 38, no. 11, Nov. 1950.
[11] B. Z. Katsenelenbaum, *Theory of Non-Regular Waveguides with Slowly Varying Parameters* (Russian). Moscow, U.S.S.R.: Academy Sci. USSR, 1961.
[12] B. A. Panchenko and E. I. Nefedov, *Microstrip Antennas* (Russian). Moscow, U.S.S.R.: Radio i Svyaz, 1986.

Mode-Matching Analysis of Circular-Ridged Waveguide Discontinuities

Uma Balaji and Ruediger Vahldieck

***Abstract*— This paper describes a mode-matching algorithm for S-parameter computation of circular-ridged waveguide (CRW) discontinuities. The ridges are shaped like the cross section of a cone (pie-shaped) with a geometry that can be described in cylindrical coordinates. This idea avoids the use of a mixed-coordinate system in the analysis of the electromagnetic fields in the ridged sections, which can, therefore, be expressed in terms of modal functions. The resulting algorithm is fast and accurate and has been utilized to design and optimize a five-section double-ridge filter and a quadruple-ridge waveguide transformer. The measured response of the filter is in good agreement with the calculated data.**

***Index Terms*—Algorithm, circular waveguides, eigenvalue.**

I. Introduction

Circular-ridged waveguide (CRW) components like filters, polarizers, orthomode transducers, etc., are important elements in subsystems for satellite communications. Low-cost design, small size, and optimum performance of these components is essential to satisfy today's stringent payload requirements. In this context, ease of manufacturing and accurate computer-aided design of CRW components are equally important issues. This paper describes the design of CRW filters and transformers in which the ridge geometry has been modified from the usual rectangular shape to a pie shape (Fig. 1) for which the geometry can be described entirely in cylindrical coordinates. This approach avoids the use of a mixed-coordinate system in the field-theory analysis of CRW structures. Thus, simplifying the algorithm without complicating the fabrication of CRW components.

In [1] and [2], the authors have presented an eigenvalue analysis of pie-shaped ridge structures in circular waveguides by using the radial mode-matching method. In that work and due to the pie shaped ridges, the electromagnetic field in the subsections of the CRW were described by modal functions. On the basis of [1] and [2], a scattering parameter analysis of double-ridged circular waveguide discontinuities was presented in [3]. To verify the algorithm, we have designed, built, and tested a five resonator double-ridged filter and found very good agreement with theoretical data.

Manuscript received October 25, 1996; revised November 21, 1997.

U. Balaji is with the Laboratory for Lightwave Electronics, Microwaves and Communications (LLMIC), Department of Electrical and Computer Engineering, University of Victoria, Victoria, B.C., Canada V8W 3P6.

R. Vahldieck is with the Swiss Federal Institute of Technology Zurich (ETHZ), Laboratory for Electromagnetic Fields and Microwave Electronics (IFH), ETH Zentrum, CH-8092, Zurich, Switzerland.

Publisher Item Identifier S 0018-9480(98)01597-X.

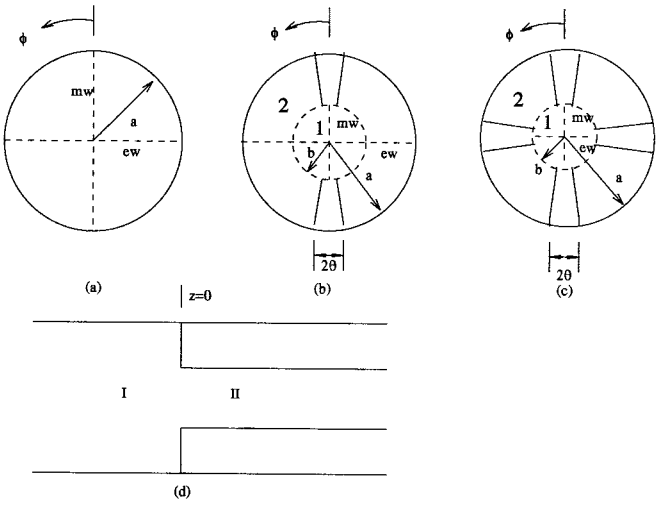

Fig. 1. Cross section of (a) circular waveguide (region I), (b) double-ridged circular waveguide (region II), (c) quadruple-ridged circular waveguide (region II), and (d) sideview of the discontinuity.

II. Theory

A mode-matching method is developed to calculate the generalized scattering matrix of a discontinuity between an empty circular waveguide and a double- or quadruple-ridged circular waveguide. The cross section of such a discontinuity is shown in Fig. 1. Region II in Fig. 1(d) can either be a double- or quadruple-ridged waveguide. Since the $\mathrm{TE}_{1,1}$ mode is the fundamental mode of propagation, a magnetic- and electric-wall symmetry can be used. The electric and magnetic potential functions in the empty circular waveguide for such a symmetry can be written as follows:

$$\psi^{(\mathrm{I}h)} = \sum_{m=1}^{M} \sum_{n=1,3}^{N} P_{n,m}^{\mathrm{I}h} J_n\left(k_{c_{n,m}}^{\mathrm{I}h}\rho\right) \sin n\phi \tag{1}$$

$$\psi^{(\mathrm{I}e)} = \sum_{m=1}^{M} \sum_{n=1,3}^{N} P_{n,m}^{\mathrm{I}e} J_n\left(k_{c_{n,m}}^{\mathrm{I}e}\rho\right) \cos n\phi. \tag{2}$$

The coefficients P represent the power normalization constants and are obtained by setting the magnitude of the power carried in each of the modes to unity. The eigenvalues of the circular waveguide for TE and TM modes can be determined from the zeros of the Bessel functions [4]. The values of M and N in (2) depend on the number of TE and TM modes used in the evaluation of the generalized scattering matrix. The electric and magnetic potential functions in the CRW (region II) can be written as a sum of those in subsections (1) and (2), shown in Fig. 1(b) or (c):

$$\psi^{(\mathrm{II}h)} = \sum_{r=1}^{R} \left(\psi^{(1h)} + \psi^{(2h)}\right) \tag{3}$$

$$\psi^{(\mathrm{II}e)} = \sum_{r=1}^{R} \left(\psi^{(1e)} + \psi^{(2e)}\right) \tag{4}$$

where $\psi^{(1h)}$ and $\psi^{(2h)}$ are given as

$$\psi^{(1h)} = \sum_{n=1,3}^{N1} A_n J_n\left(k_{c_r}^{\mathrm{II}h}\rho\right)\sin n\phi \tag{5}$$

$$\psi^{(2h)} = \sum_{m=0}^{N2} C_m\left[N_l'\left(k_{c_r}^{\mathrm{II}h}a\right)J_l\left(k_{c_r}^{\mathrm{II}h}\rho\right) - J_l'\left(k_{c_r}^{\mathrm{II}h}a\right)N_l\left(k_{c_r}^{\mathrm{II}h}\rho\right)\right]\cos l(\phi-\theta) \tag{6}$$

where $l = m\pi/\frac{\pi}{2} - \theta$ for a double-ridged cross section with ridge thickness of 2θ and for the quadruple-ridged cross section $l = m\pi/\frac{\pi}{2} - 2\theta$. It should be noted that the orders of the Bessel and Neumann functions used in the potential functions are nonintegers in the ridged circular waveguide subsection (2). Similarly $\psi^{(1e)}$ and $\psi^{(2e)}$ in subsection (2) are written as

$$\psi^{(1e)} = \sum_{n=1,3}^{N1} B_n J_n\left(k_{c_r}^{\mathrm{II}e}\rho\right)\cos n\phi \tag{7}$$

$$\psi^{(2e)} = \sum_{m=1}^{N2} D_m\left[N_l\left(k_{c_r}^{\mathrm{II}e}a\right)J_l\left(k_{c_r}^{\mathrm{II}e}\rho\right) - J_l\left(k_{c_r}^{\mathrm{II}e}a\right)N_l\left(k_{c_r}^{\mathrm{II}e}\rho\right)\right]\sin l(\phi-\theta). \tag{8}$$

The procedure to determine the eigenvalues and the amplitude coefficients in the above equations have been described in [1] and [2]. The amplitude coefficients are once again power normalized so that the magnitude of the power carried in each of the modes is unity. For thin ridges, the number of expansion terms ($N1$ and $N2$) in the two subsections are chosen equal and these values, along with R, depend on the number of TE and TM modes necessary to achieve convergence of the S-parameters.

From the potential functions described above in the two regions of discontinuity, the electric and magnetic fields in each of the regions of Fig. 1 can be derived. At the interface of the two regions ($z = 0$), the continuity of the tangential E- and H-field components of the incident and reflected waves can be written as

$$\begin{aligned} E_T^{\mathrm{I}} = E_T^{(\mathrm{II})}, \quad & r \in [0,b],\ \phi \in [0,2\pi] \text{ and} \\ & r \in [b,a],\ \phi \in [(\theta,\pi-\theta);(\pi+\theta,2\pi-\theta)] \\ = 0, \quad & r \in [b,a],\ \phi \in [-\theta,+\theta] \text{ and } \phi \in [\pi-\theta,\pi+\theta] \end{aligned} \tag{9}$$

$$H_T^{\mathrm{I}} = H_T^{(\mathrm{II})}, \quad r \in [0,b], \phi \in [0,2\pi] \text{ and } r \in [b,a],\ \phi \in [(\theta,\pi-\theta);(\pi+\theta,2\pi-\theta)]$$

where the superscript represent the appropriate regions in the discontinuity. Using the orthogonality property of the modes, the above equation results in four sets of equations relating the unknown wave amplitudes of the incident (F) and reflected (B) waves. For instance, the continuity of the tangential components of the E-field results in the two sets of equations given below:

$$(F^{\mathrm{I}h} + B^{\mathrm{I}h}) = [L_{HH}](F^{\mathrm{II}h} + B^{\mathrm{II}h}) \tag{10}$$

$$(F^{\mathrm{I}e} + B^{\mathrm{I}e}) = [L_{EE}](F^{\mathrm{II}e} + B^{\mathrm{II}e}) + [L_{EH}](F^{\mathrm{II}h} + B^{\mathrm{II}h}) \tag{11}$$

where the $[L]$ matrices give the coupling between the fundamental and higher order TE and TM modes. The integrals of these $[L]$ matrices are given in the Appendix. While some of the integrals can be evaluated analytically [4], some others are evaluated numerically. However, all the coupling integrals are frequency independent and, hence, the numerical integration is not repeated at every frequency point. The continuity of the tangential components of the H-field results in coupling matrices that are the transposed matrices of the coupling matrices in (10) and (11) with the sets of equations given below:

$$(F^{\mathrm{II}e} - B^{\mathrm{II}e}) = \left[L_{EE}^T\right](F^{\mathrm{I}e} - B^{\mathrm{I}e}) \tag{12}$$

$$(F^{\mathrm{II}h} - B^{\mathrm{II}h}) = \left[L_{HH}^T\right](F^{\mathrm{I}h} - B^{\mathrm{I}h}) + \left[L_{EH}^T\right](F^{\mathrm{I}e} - B^{\mathrm{I}e}). \tag{13}$$

Suitable algebraic operations on the matrix equations in (10)–(13) yields the generalized scattering matrix of the discontinuity.

Structures like evanescent-mode filters also involve a step discontinuity between two axially symmetric circular waveguides. For such a discontinuity it is usually sufficient to use only $\mathrm{TE}_{1,n}$ and $\mathrm{TM}_{1,n}$ modes. However, since subsequent discontinuities contain ridged waveguide sections in which $\mathrm{TE}_{2m+1,n}$ and $\mathrm{TM}_{2m+1,n}$ modes are excited, these modes must also be considered as excitation terms for the first discontinuity. Hence, the generalized scattering matrix of a step discontinuity from above to below cutoff waveguide should be calculated using a sufficient number of $\mathrm{TE}_{2m+1,n}$ and $\mathrm{TM}_{2m+1,n}$ modes. By cascading the generalized scattering matrices at various step discontinuities, the generalized S-matrix of the matching networks or the evanescent-mode filters is obtained.

III. Results

The transition from an empty circular waveguide to a double-ridged circular waveguide and a symmetric iris step in circular waveguide have been validated in [3]. Good agreement was found with the measurements when 40 TE and TM modes were used in the analysis. On the basis of the above investigation, a three-section Chebyshev transformer in a double-ridged circular waveguide and a three-resonator evanescent-mode filter was designed and presented in [3].

A quadruple-ridged circular waveguide transformer has been designed and optimized here. Its response is shown in Fig. 2. The optimization with respect to the lengths of the transformer sections was performed with 20 modes and a final analysis was done with 40 TE and TM modes. In order to improve the bandwidth of the transformer, the outer circular diameter (dimension a in Fig. 1) of the quadruple-ridged waveguide was reduced. As a result, the cutoff frequency of the next higher mode ($\mathrm{TE}_{3,1}$) which limits the bandwidth of the transformer is increased and, thus, also the bandwidth of the transformer, as illustrated in Fig. 3.

A five resonator evanescent-mode filter has also been designed, optimized, and fabricated. The number of the TE and TM modes used during the optimization was 30. In the final analysis of the filter, 40 modes were included. The 0.003-in uniformly thick copper sheet used in the practical realization was approximated as $\theta = 5.5^\circ$. The passband and stopband response of the calculated and realized filter is shown in Fig. 4. Good agreement with measurements was found. The high insertion loss of 2.5 dB in the passband of the filter was mainly due to the impedance mismatch at the input to the filter and the fact that the fabrication tolerances of the ridges are too high. The wide-band response of the CRW filter behaves similar to an evanescent-mode filter in a rectangular waveguide.

IV. Conclusion

This paper has introduced a mode-matching technique for field-theory design of CRW components like filters and impedance transformers. Fundamental and higher order mode interaction at and

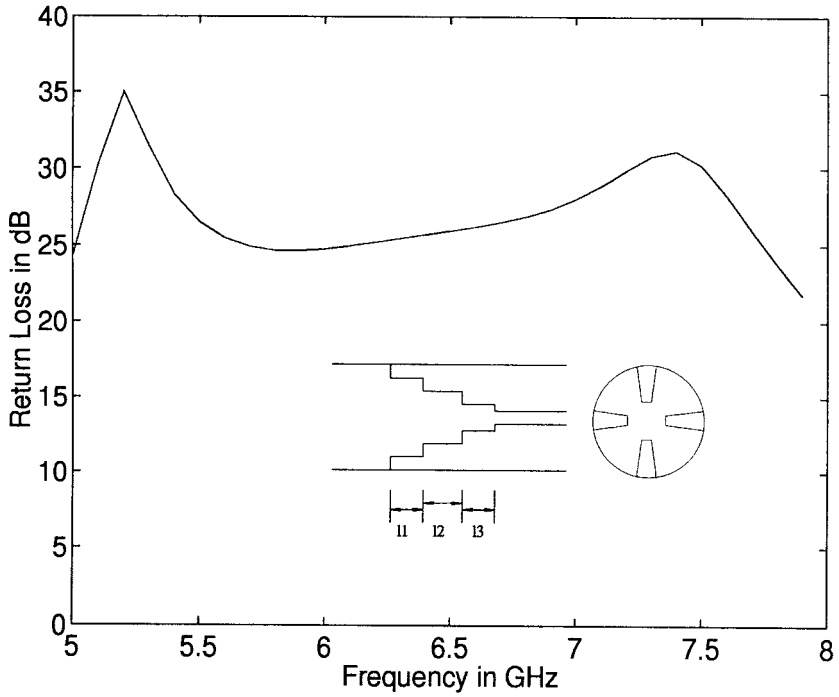

Fig. 2. Response of an optimum three-section quadruple-ridged circular waveguide transformer (dimensions in centimeters, $\theta = 5^\circ$ for all sections). Section 1: $a = 2$, $b = 1.62$, $11 = 1.519$, Section 2: $a = 2$, $b = 1.09$, $12 = 1.404$, Section 3: $a = 2$, $b = 0.68$, $13 = 1.363$, Section 4: $a = 2$, $b = 0.5$.

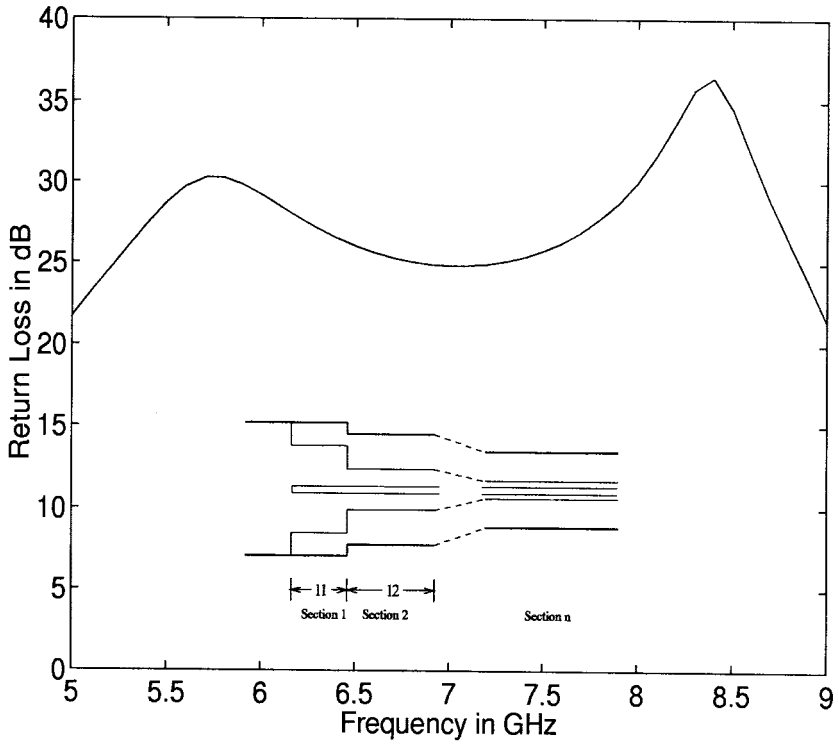

Fig. 3. Response of an optimum three-section quadruple-ridged circular waveguide transformer with tapered circular waveguide housing (dimensions in centimeters, $\theta = 5^\circ$ for all sections). Section 1: $a = 2$, $b = 1.7$, $11 = 1.162$, Section 2: $a = 1.95$, $b = 1.45$, $12 = 1.474$, Section 3: $a = 1.9$, $b = 1.25$, $13 = 1.59$, Section 4: $a = 1.85$, $b = 1.2$.

between discontinuities has been taken into account. An evanescent-mode filter in circular waveguide technology has been designed and measured. It is found that for large penetration depths of the ridge a uniformly thick ridge can be approximated with an angle subtended by the tip of the ridge. The technique used in this paper shows that the method is suitable for component design in CRW's.

APPENDIX

The integrals of the coupling matrices L are given below:

$$L_{HH}(x,y) = \sum_{n=1,3}^{N1} (Term_1 + Term_2)\sqrt{\frac{k_z^{1h}(x)}{k_z^{11h}(y)}} \tag{14}$$

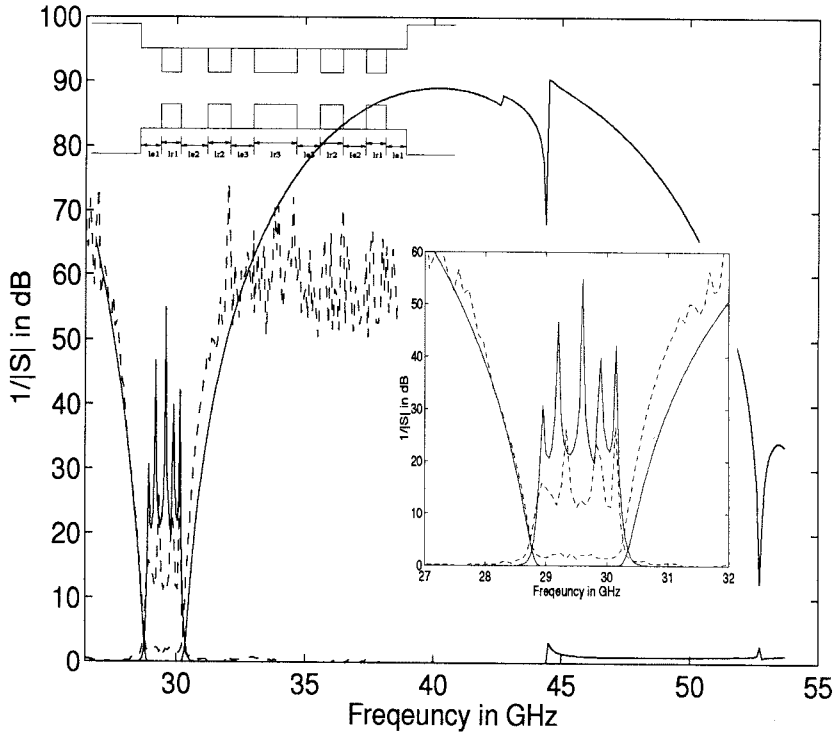

Fig. 4. Response of an optimum five-resonator evanescent-mode circular waveguide filter of dimensions shown in Fig. 9. Solid lines: computed response, dashed line: measured response.

where the *Term*$_1$ and *Term*$_2$ are given below. The x corresponds to the number of the mode that is excited in cross-section I, while y corresponds to that in II. Also, k_z represent the propagation constants in regions I and II of the corresponding modes and is evaluated from k_o (the propagation constant in free space) and the eigenvalues k_c of the respective modes:

Term$_1$

$$= P^{\mathrm{I}h}_{s,p} P^{\mathrm{II}h}_{n,r} \pi A_n \int_0^b \left[\frac{ns}{\rho^2} J_s\left(k^{\mathrm{I}h}_{c_{s,p}} \rho\right) J_n\left(k^{\mathrm{II}h}_{c_r} \rho\right) + J'_s\left(k^{\mathrm{I}h}_{c_{s,p}} \rho\right) \cdot J'_n\left(k^{\mathrm{II}h}_{c_r} \rho\right) \right] \rho \, d\rho, \qquad \text{if } n = s$$

$$= 0, \qquad \text{if } n \neq s \tag{15}$$

Term$_2$

$$= P^{\mathrm{I}h}_{s,p} P^{\mathrm{II}h}_{n,r} C_n \int_b^a -\frac{ls}{\rho^2} J_s\left(k^{\mathrm{I}h}_{c_{s,p}} \rho\right) \left[J_l\left(k^{\mathrm{II}h}_{c_r} \rho\right) N'_l\left(k^{\mathrm{II}h}_{c_r} a\right) - J'_l\left(k^{\mathrm{II}h}_{c_r} a\right) N_l\left(k^{\mathrm{II}h}_{c_r} \rho\right) \right]$$
$$\cdot \rho \, d\rho \times 4 \int_\theta^{\frac{\pi}{2}} \cos s\phi \sin l(\phi - \theta) \, d\phi + P^{\mathrm{I}h}_{s,p} P^{\mathrm{II}h}_{n,r} C_n$$
$$\cdot \int_b^a J'_s\left(k^{\mathrm{I}h}_{c_{s,p}} \rho\right) \left[J'_l\left(k^{\mathrm{II}h}_{c_r} \rho\right) N'_l\left(k^{\mathrm{II}h}_{c_r} a\right) - J'_l\left(k^{\mathrm{II}h}_{c_r} a\right) N'_l\left(k^{\mathrm{II}h}_{c_r} \rho\right) \right]$$
$$\cdot \rho \, d\rho \times 4 \int_\theta^{\frac{\pi}{2}} \sin s\phi \cos l(\phi - \theta) \, d\phi \tag{16}$$

where $l = (n-1)\pi/2\phi_0$; $\phi_0 = (\pi/2 - \theta)$ for double-ridged circular waveguide in region II and $\phi_0 = (\pi/2 - 2\theta)$ for quadruple-ridged circular waveguide in region II. The value of ϕ_o used in the subsequent equations remains as mentioned above for the double- and quadruple-ridged circular waveguide. Also, for the quadruple-ridged circular waveguide, the upper limit of the ϕ integral in *Term*$_2$ is $(\pi/2 - 0)$. This change is also applicable to the following equations for *Term*$_4$ and *Term*$_6$ in the analysis of a quadruple-ridged waveguide discontinuity

$$L_{EE}(x,y) = \sum_{n=1,3}^{N1} (\mathit{Term}_3 + \mathit{Term}_4) \sqrt{\frac{k^{\mathrm{II}e}_z(x)}{k^{\mathrm{I}e}_z(y)}} \tag{17}$$

Term$_3$

$$= P^{\mathrm{I}e}_{s,p} P^{\mathrm{II}e}_{n,r} \pi B_n \int_0^b \left[\frac{ns}{\rho^2} J_s\left(k^{\mathrm{I}e}_{c_{s,p}} \rho\right) J_n\left(k^{\mathrm{II}e}_{c_r} \rho\right) + J'_s\left(k^{\mathrm{I}e}_{c_{s,p}} \rho\right) \cdot J'_n\left(k^{\mathrm{II}e}_{c_r} \rho\right) \right] \rho \, d\rho, \qquad \text{if } n = s$$

$$= 0, \qquad \text{if } n \neq s \tag{18}$$

Term$_4$

$$= P^{\mathrm{I}e}_{s,p} P^{\mathrm{II}e}_{n,r} D_n \int_b^a -\frac{ls}{\rho^2} J_s\left(k^{\mathrm{I}e}_{c_{s,p}} \rho\right) \left[J_l\left(k^{\mathrm{II}e}_{c_r} \rho\right) N_l\left(k^{\mathrm{II}e}_{c_r} a\right) - J_l\left(k^{\mathrm{II}e}_{c_r} a\right) N_l\left(k^{\mathrm{II}e}_{c_r} \rho\right) \right]$$
$$\cdot \rho \, d\rho \times 4 \int_\theta^{\frac{\pi}{2}} \sin s\phi \cos l(\phi - \theta) \, d\phi$$
$$+ P^{\mathrm{I}e}_{s,p} P^{\mathrm{II}e}_{n,r} D_n \int_b^a J'_s\left(k^{\mathrm{I}e}_{c_{s,p}} \rho\right) \left[J'_l\left(k^{\mathrm{II}e}_{c_r} \rho\right) N_l\left(k^{\mathrm{II}e}_{c_r} a\right) - J_l\left(k^{\mathrm{II}e}_{c_r} a\right) N'_l\left(k^{\mathrm{II}e}_{c_r} \rho\right) \right]$$
$$\cdot \rho \, d\rho \times 4 \int_\theta^{\frac{\pi}{2}} \cos s\phi \sin l(\phi - \theta) \, d\phi \tag{19}$$

where $l = (n+1)\pi/\phi_o$.

$$L_{EH}(x,y) = \sum_{n=1,3}^{N1} (\mathit{Term}_5 + \mathit{Term}_6) \frac{k_o}{\sqrt{k^{\mathrm{II}h}_z(y) k^{\mathrm{I}e}_z(x)}} \tag{20}$$

$$\begin{aligned}\textit{Term}_5 =& P^{\mathrm{I}e}_{s,p}P^{\mathrm{II}h}_{n,r}\pi A_n\int_0^b \left[nJ'_s\left(k^{\mathrm{I}e}_{c_{s,p}}\rho\right)J_n\left(k^{\mathrm{II}h}_{c_r}\rho\right)+sJ_s\left(k^{\mathrm{I}e}_{c_r}\rho\right)\right.\\ &\left.\cdot J'_n\left(k^{\mathrm{II}h}_{c}\rho\right)\right]d\rho, \qquad \text{if } n=s\\ =&0, \qquad \text{if } n\neq s \end{aligned} \tag{21}$$

$$\begin{aligned}\textit{Term}_6 =& P^{\mathrm{I}e}_{s,p}P^{\mathrm{II}h}_{n,r}C_n\int_b^a -lJ'_s\left(k^{\mathrm{I}e}_{c_{s,p}}\rho\right)\left[J_l\left(k^{\mathrm{II}h}_{c_r}\rho\right)N'_l\left(k^{\mathrm{II}h}_{c_r}a\right)\right.\\ &\left.-J'_l\left(k^{\mathrm{II}h}_{c_r}a\right)N_l\left(k^{\mathrm{II}h}_{c_r}\rho\right)\right]\\ &\cdot d\rho\times 4\int_\theta^{\frac{\pi}{2}}\cos s\phi\sin l(\phi-\theta)\,d\phi + P^{\mathrm{I}e}_{s,p}P^{\mathrm{II}h}_{n,r}C_n\\ &\cdot\int_b^a sJ_s\left(k^{\mathrm{I}e}_{c_{s,p}}\rho\right)\left[J'_l\left(k^{\mathrm{II}h}_{c_r}\rho\right)N'_l\left(k^{\mathrm{II}h}_{c_r}a\right)-J'_l\left(k^{\mathrm{II}h}_{c_r}a\right)\right.\\ &\left.\cdot N'_l\left(k^{\mathrm{II}h}_{c_r}\rho\right)\right]\\ &\cdot d\rho\times 4\int_\theta^{\frac{\pi}{2}}\sin s\phi\cos l(\phi-\theta)\,d\phi \end{aligned} \tag{22}$$

where $l = (n-1)\pi/\phi_o$.

References

[1] U. Balaji and R. Vahldieck, "Radial mode matching analysis of ridged circular waveguide," in *IEEE MTT-S Dig.*, Orlando, FL, May 1995, pp. 637–640.

[2] ——, "Radial mode matching analysis of ridged circular waveguides," *IEEE Trans. Microwave Theory Tech.*, vol. 44, pp. 1183–1186, July 1996.

[3] ——, "Field theory based S-parameter analysis of circular ridged waveguide discontinuities," in *IEEE MTT-S Dig.*, San Francisco, CA, June 1996, pp. 1853–1856.

[4] S. Ramo, J. R. Whinnery, and T. Van Duzer, *Fields and Waves in Communication Electronics*. New York: Wiley, 1965.

Simple Determination of All Capacitances for a Set of Parallel Microstrip Lines

Florian Sellberg

***Abstract*— A fast and moderately accurate method to describe the complicated dependence on design and process parameters of coupling capacitances between a set of parallel lines is presented in this paper. It involves only one circuit-dependent parameter at a time. This is accomplished by calculating the capacitance coefficient matrix through inversion of a potential coefficient matrix with much simpler dependence on geometry. Self elements are approximately independent of the presence of other lines, and mutual elements do not depend on linewidths or interfering lines as long as the ground is sufficiently far away. The potential coefficients are derived by inverting one- or two-line capacitance matrices that are either theoretically calculated or determined by measurements on integrated circuit (IC) test structures. Look-up tables for a specific IC process can then be constructed with only linewidth as the parameter for self potential elements and distance between line centers as parameter for mutual potential elements. General algorithms have been derived for microstrip on one or two layers of dielectric.**

***Index Terms*— Coupled lines, design automation software, wiring models.**

Manuscript received February 13, 1997; revised November 21, 1997. This work was supported by NUTEK under the High Speed Electronics Consortium Project 9 302 955.

The author is with IMC-Industrial Microelectronics Center, S-16440 Kista, Sweden (e-mail: florian@imc.kth.se).

Publisher Item Identifier S 0018-9480(98)01598-1.

I. Introduction

As digital and mixed analog/digital integrated circuits (IC's) move higher and higher in speed and increase in size, complexity, and packing density, the need rises to include moderately accurate models of line-to-line and line-to-ground capacitances for the estimation of performance degradation and crosstalk. When line length is not negligible compared to wavelength, inductances must also be taken into account. Much work has been devoted to alleviate the burden on computers due to the inclusion of parasitic elements in the circuit simulators [1]. Separate programs for evaluation of parallel lines are available [2]. One recent work [3] describes the generation of analytical models for interconnect capacitances in the form of polynomials in the design parameters given the values of process parameters. Contrary to the method described in this paper, every addition of another line necessitates the determination of a new set of curves with a rapid increase in the number of parameters (N lines give $2N-1$ parameters).

Our method is based on the observation that parallel lines propagating TEM waves are described by an inductance matrix with—to a first approximation—self elements depending only on the perimeter of the line cross section, and mutual elements depending only on the distance between line centers, without being influenced by the addition of new lines, whether shielding or not. The capacitance matrix is derived by inversion of the complete inductance matrix for the set of N lines. With inhomogeneous dielectric outside the conductors, wave propagation is quasi-TEM, and this simple relation breaks down. It is found, though, that the elements of the potential coefficient matrix (the inverse of the capacitance coefficient matrix) show the same simple dependence on design parameters as do the inductance elements.

II. General TEM Relations

For a set of N parallel conductors over a ground surface and propagating TEM waves, one can define inductances (self and mutual) and capacitances between conductors. The inductance matrix is $\mu_0[L_{ij}]$ H/m and the capacitance coefficient matrix is $\varepsilon_0[c_{ij}]$ F/m, both of rank $N\times N$. If the whole space outside the conductors is filled with a dielectric with permittivity ε, the following well-known relation is true:

$$[c_{ij}] = \varepsilon[L_{ij}]^{-1}. \tag{1}$$

The physical capacitances per unit line length (normalized to ε_0) between conductor i and ground C_{i0} and between conductors i and j, C_{ij} are connected to the capacitance coefficients

$$\begin{aligned} C_{i0} &= \Sigma_j c_{ij} \\ C_{ij} &= -c_{ij}, \qquad \text{with } i\neq j. \end{aligned} \tag{1a}$$

In a strict sense, (1) is true only when the currents are confined to the surface of the conductors (infinite conductivity)—or when the distance between conductors and to the ground surface is much larger than their transverse dimensions.

III. Self-Inductance

For a single conductor over a ground plane, the inductance per unit length depends on one dimensionless variable: the transverse perimeter length of the conductor divided by the distance between some point in the conductor and the ground plane. The addition of